REPORT DOCUMENTATION PAGE

Form Approved

OMB No. 0704-0188

1. REPORT DATE *(DD-MM-YYYY)*	2. REPORT TYPE	3. DATES COVERED *(From - To)*
20-Oct-14	Final	14-Jun-12 to 13-Jun-13

4. TITLE AND SUBTITLE

Effects of Molecular Stresses on Energy Transfer Pathways in Opto- and Electro-Excited Conjugated Polymers for High-Efficiency Optoelectronic Devices

5a. CONTRACT NUMBER
FA2386-12-1-4064

5b. GRANT NUMBER
Grant AOARD-124064

5c. PROGRAM ELEMENT NUMBER
61102F

6. AUTHOR(S)

Prof. Arnold Chang-Mou Yang

5d. PROJECT NUMBER

5e. TASK NUMBER

5f. WORK UNIT NUMBER

7. PERFORMING ORGANIZATION NAME(S) AND ADDRESS(ES)

National Tsing Hua University
101, Kuang Fu Rd, Sec 2
Hsinchu 30043
Taiwan

8. PERFORMING ORGANIZATION REPORT NUMBER

N/A

9. SPONSORING/MONITORING AGENCY NAME(S) AND ADDRESS(ES)

AOARD
UNIT 45002
APO AP 96338-5002

10. SPONSOR/MONITOR'S ACRONYM(S)

AFRL/AFOSR/IOA(AOARD)

11. SPONSOR/MONITOR'S REPORT NUMBER(S)

AOARD-124064

12. DISTRIBUTION/AVAILABILITY STATEMENT

Distribution A: Approved for public release. Distribution is unlimited.

13. SUPPLEMENTARY NOTES

14. ABSTRACT

The role of mechanical stresses in the optoelectronic behavior and exciton formation of conjugated polymers was explored in order to understand and to exploit the massive efficiency enhancements produced by mechanical stretching. The molecular chains of conjugated polymer MEH-PPV were mechanically stretched by capillary forces via the dewetting process induced by solvent annealing rather than thermal annealing in order to rid of the potential effects of thermal degradation and to open the possibility for industrial applications. Similar results of photoluminescence enhancements, about two orders of magnitude increases, were obtained as those by thermal dewetting, indicating that capillary force indeed can be used to stretch the polymer chains for the purpose of efficiency enhancements. These blue shifts were proved to be due to molecular kinks that resulted from molecular flows of the entangled macromolecules. Poor solvents produced even greater chain stretching effects than with good solvents, a result attributed to reduced stress relaxation during the dewetting process. Stretching enacted by capillary forces required full penetration of the solvent into the whole film, indicating that interfacial adhesion to the substrate can effectively constrain movement of confined polymer chains. As revealed by temperature effects stretching-induced efficiency enhancements were found to accompany a decrease in the Huang-Rhays parameter, which is a key identifier of electron-phonon coupling. In addition, as revealed by the up-conversion confocal experiments, energy decay in the ultrafast regime (< 10 ps) was found to slow remarkably in stretched polymer chains residing in the dewetting droplets. A separate experiment of stretching graphene-containing MEH-PPV films was performed to check the effect of mechanical stretching on heterojunction quenching. It was found that mechanical stretching indeed can reduce the heterojunction quenching, in consistency with the observations involving the dewetting residual layer. Hence, mechanical interactions should play a fundamental role in the formation and behavior of excitons in conjugated polymers. Finally, the mechanical stretching effect was reproduced when conjugated polymer chains were constrained by intermolecular hydrogen bonding and thus leads

to suppression of electron-phonon interactions.

15. SUBJECT TERMS

Conductive Polymers, nano photonics, Graphene

16. SECURITY CLASSIFICATION OF:			17. LIMITATION OF ABSTRACT	18. NUMBER OF PAGES	19a. NAME OF RESPONSIBLE PERSON
a. REPORT	b. ABSTRACT	c. THIS PAGE			Kenneth Caster, Ph.D.
U	U	U	SAR	25	19b. TELEPHONE NUMBER *(Include area code)* +81-42-511-2000

Final Report for AOARD 124064

Effects of Molecular Stresses on Energy Transfer Pathways in Opto- and Electro-Excited Conjugated Polymers for High-Efficiency Optoelectronic Devices

Name of Principal Investigators: Arnold Chang-Mou Yang

- e-mail address : acyang@mse.nthu.edu.tw
- Institution : Department of Materials Science and Engineering, National Tsing Hua University, Hsinchu, Taiwan
- Mailing Address : 101, Kuang Fu Road, Hsinchu City, Taiwan
- Phone : +886 (3) 572 0792
- Fax : +886 (3) 572 2366

Period of Performance: 07/01/2012 – 06/14/2013

Abstract:

The role of mechanical stresses in the optoelectronic behavior and exciton formation of conjugated polymers was explored in order to understand and to exploit the massive efficiency enhancements produced by mechanical stretching. The molecular chains of conjugated polymer MEH-PPV were mechanically stretched by capillary forces via the dewetting process induced by solvent annealing rather than thermal annealing in order to rid of the potential effects of thermal degradation and to open the possibility for industrial applications. Similar results of PL enhancements, about two orders of magnitude increases, were obtained as those by thermal dewetting, indicating that capillary force indeed can be used to stretch the polymer chains for the purpose of efficiency enhancements. The blue shifts associated with the efficiency enhancements were proved to be due to molecular kinks resulted from molecular flows of the entangled macromolecules. Poorer solvents produced even greater chain stretching effects than the good solvent, a result attributed to reduced stress relaxation during the dewetting process. The stretching enacted by the capillary force required full penetration of the solvent of the whole film, indicating that interfacial adhesion to the substrate can effectively constrain the movements of the confined polymer chains. The stretching-induced efficiency enhancements were found to accompany with a decrease of Huang-Rhays parameter, a key parameter of the electron-phonon coupling, as revealed by the temperature effect. In addition, as revealed by the up-conversion confocal experiments, the energy decay in the ultrafast regime (< 10 ps) was found to slow remarkably in the stretched polymer chains residing in the dewetting droplets. A separate experiment of stretching graphene-containing MEH-PPV films was carried out to check the effect of mechanical stretching on heterojunction quenching. It was found that mechanical stretching indeed can reduce the heterojunction quenching, in consistency with the observations involving the dewetting residual layer. Hence, mechanical interactions should play a fundamental role in the formation and behavior of excitons in conjugated polymers. Finally, the mechanical stretching effect can be reproduced when the conjugated polymer chains were constrained by intermolecular hydrogen bonding that have effectively constrained the polymer backbones to suppress the electron-phonon interactions.

Introduction:

Due to low carbon footprints and advantageous combination of properties, conjugated polymers have attracted broad interests for active roles in future optoelectronics,

semiconductors, and renewable energies. However, the low optoelectronic efficiencies, short service life, and inferior electric conductivity have been obstructing their prevalent applications. Recently, important clues emerged that variation of the molecular conformation, mostly in the single molecular state in liquid or solid solutions, may lead to dramatic changes in the quantum efficiencies. However, the fact that solid films generally manifest far less efficiencies compared to solutions even for similar chain conformations poses a serious problem for the theory based on molecular conformation.

Against this backdrop, our group has demonstrated that mechanical stretching conjugated polymer strands may produce dramatic efficiency enhancements. The effect was attributed to the suppression of exciton-phonon coupling that ordinarily leads to exciton trapping and low efficiencies. For the free standing films containing MEH-PPV molecules that were stretched forming local deformation zones, dramatic enhancements of around 1-2 order of magnitude were observed. Similarly, by dewetting the ultrathin polymer film containing MEH-PPV we also observed the tremendous increase of the quantum efficiencies by a factor about tens folds due to the pulling of the molecules during the mass re-distribution. We also have since been trying to clarify the role of stresses, in differentiation to strains, for efficiency enhancements. In addition, we studied the stress effect in simplified systems of single-molecular layers. Moreover, we have unveiled the stress effect on charge conductivity.

In this work, we continued to consolidate our proposal of the stress effect by working in a) Solvent dewetting experiment to complement the thermal dewetting experiments, b) Temperature-Varying experiments to probe the dynamics of de-excitation, c) Stretching-induced de-quenching on graphene surface to verify the residual layer observations, d) Imprinting experiments to explore other feasible method for applications, e) Intermolecular H-bonding experiment to test the effect of molecular constraintsd, f) Light-induced molecular changes to check the stress effect in a reciprocal fashion, g) Ultrafast PL experiment to probe the clues of phonon intervention in the exciton formation and properties, and h) Device making. The results are presented in the following sections.

Experiments, Results and Discussions:

1. Paradoxical Excitons in Conjugated Polymers: the Role of Mechanical Interactions

The theoretical basis of our understanding on the optoelectronic behavior of conjugated polymers lies on our knowledge of how the photo-excited states, i.e., the so-called "excitons" are formed in conjugated polymers. Well developed in the systems of inorganic crystals, excitons are the photo-generated electron-hole pairs bounded by electrostatic attraction in between.

However, in a sharp contrast to the inorganic crystalline materials where only a small fraction of photo-generated electron-hole pairs are formed as a result of optical excitation, excitons predominate all the photo-excited species in conjugated polymers. The underlying reason remains obscure.

Intriguingly, furthermore, excitons in the inorganic crystalline materials can be categorized into two types: the Wannier-Mott excitons (i.e., the free excitons) and the Frenckel excitons (i.e., the tightly bounded excitons (Fig. 1a and 1b). For the free-moving delocalized states of the Wannier-Mott excitons, the binding energy in silicon, for example, is around ~0.01 eV, highly unstable in the ambient condition of room temperature. Consistent to the weak bounding state, the radii of the delocalized species typically encompass many unit cells and typically exist in materials of **s**mall bandgap and large dielectric constant. In converse, the the tightly bounded Frenkel excitons are immobile, with a large binding energy ranging from 0.1 eV to 1 eV), and localized within a radius comparable to the unit cell (~0.2-0.3 nm). They are typically induced in materials of large

band gap and small dielectric constant. In contrast, for conjugated polymers, the excitons are generally immobile, and hence are commonly classified as the Frenkel exciton. However, the separation between the charges is large, around 6-8 monomer (~3 nm). A question arises: are the binding energies that are based on Coulomb interactions large enough for accounting the observed exciton behavior in conjugated polymers? The answer clearly is no.

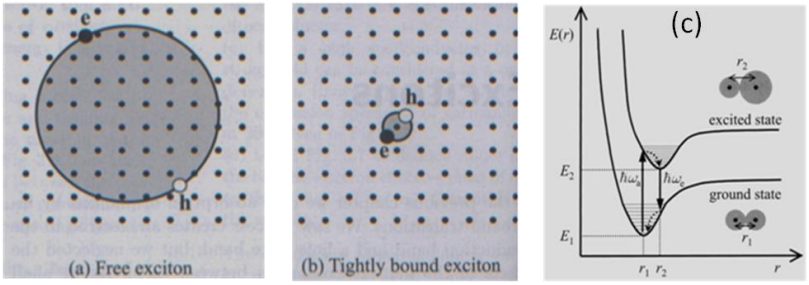

Figure 1. Schematic depiction of the a) free exciton, b) tightly bound exciton, and c) the Franck-Condon cycles.

The key to resolve the paradoxical question may lie in the interactions between the excited electronic states and the local molecular deformation of conjugated polymers. Following the classical Franck-Condon principle in inorganic materials, the excitation process in the organic molecules can be regarded as: changes in the electron cloud spatial distribution occur immediately after photon absorption, which lead to, with a time lag, variations of the spatial arrangement of the backbone nuclei in order to minimize the free energy (Born-Oppenheimer approximation). Similarly, following the de-excitation of charge recombination that emit light, changes in the electron clouds also precede that of the nuclei spatial arrangements. The combination of these excitation and de-excitation steps constitutes the so-called Franck-Condon cycle (Fig. 1c). Obviously, the Franck-Condon cycle assumes a strong electron-phonon coupling. In the di-atomic analogy, excitations of the molecule generally lead to increases of the spatial dimensions of the molecular orbitals. Inter-atomic separation thus increases driven by elevation of the electrostatic repulsion upon excitation. Likewise, the atomic spacing decreases upon de-excitation), returning to pre-excitation state. In this fashion, the molecular dimension varies via the phonon-assisted energy dissipation.

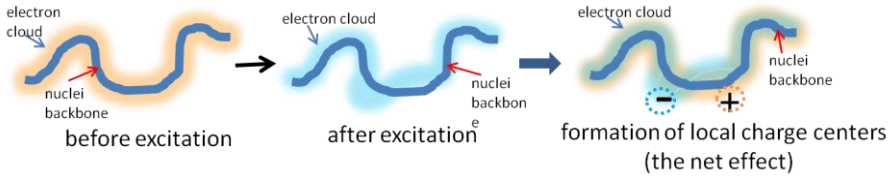

Figure 2. Schematic depiction of the coupling of photoexcitation and local molecular deformations in a section of molecular strand.

Figure 3. Schematic depiction of the suppression of molecular deformations in the stretched state.

Hence, clearly, for a molecular segment (where the coherent movements of valence electrons prevail ~conjugation length), excitations of the electron orbitals lead to the formation of electron-rich (negative-charged) and electron-poor (positive-charged) centers (Fig. 2). The increase of electrostatic interactions around the charge center force the nuclei to adjust spatial arrangement, via time-integrated torsional vibration, to minimize the local free

energy. Local molecular deformations thus arise. The local molecular deformation around a charge center tends to trap the charge unless it hops, and lead to obstructed recombination for PL or charge separation for solar cells and the reduced quantum efficiencies of the optoelectronic processes. For conjugated polymers, the strand lengthens or shortens by bond rotations. In the locally lengthened and constrained state (i.e., under a tensile stress in the molecular length scale), the degree of freedom in rotation is reduced. Therefore, the efficiency is expected to increase under the molecular tensile stresses.

There are many ways to stretch conjugated polymer strands in order to examine this stress-induced efficiency enhancement. For example, we can 1) simple tension of free standing films, 2) Molecular flows induced by capillary forces in ultrathin films, 3) Imprinting, 4) Phase separation (include. crystallization) induced stresses, 5) Multi-Layer stress transfer, 6) Residual stresses, and 7) Molecular constraints by H-bonding. In the following, some of these methods were used to explore the stress-induced effects.

2. Stretching by Capillary-Molecular Flows

A. Dewetting by Thermal Annealing:

As illustrated in our past work which was published in ACS Nano 2013, dewetting of ultrathin films destabilized by thermal annealing (Fig. 4) can lead to dramatic PL enhancements (Fig. 5 and Table 1). Dewetting of ultrathin films is effectively a fragmentation process transferring an intact film into droplets and a "residual layer" on substrate and is driven by residual stresses and capillary forces. Annealing is necessary for speeded observation: Thermal annealing or solvent vapor imbibing. The residual layer thickness was determined to be ~2-3 nm (by x-ray reflectivity and AFM).

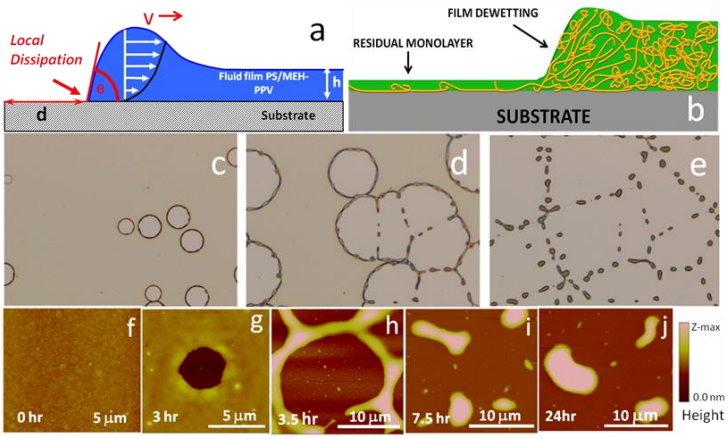

Figure 4. (a,b) Schematic depiction of the the dewetting process in a side-view. (c-e) OM observation of the dewetting on silicon substrate for a MEH-PPV/PS film. (f-j) AFM topographic micrographs for the MEH-PPV/PS film during the process of dewetting.

The dramatic enhancements in PL were accompanying the molecular flows, with a blue shift (Fig. 6). The efficiency enhancements and the blue shifts increased strongly in smaller film thicknesses, owing to increases of residual stresses and capillary force in the thinner films (Table 1).

During the annealing prior to the PL enhancement, a decrease of PL with a clear red shift occurred (Fig. 5), obviously arising from chain relaxation that led to molecular aggregation and decreases of stresses. In view of the fast decay of the residual stresses**,** capillary force apparently played the major role in the molecular flows that form the droplets and residual layer. Hence, stretched molecules could be found in the residual layer as well as the droplets.

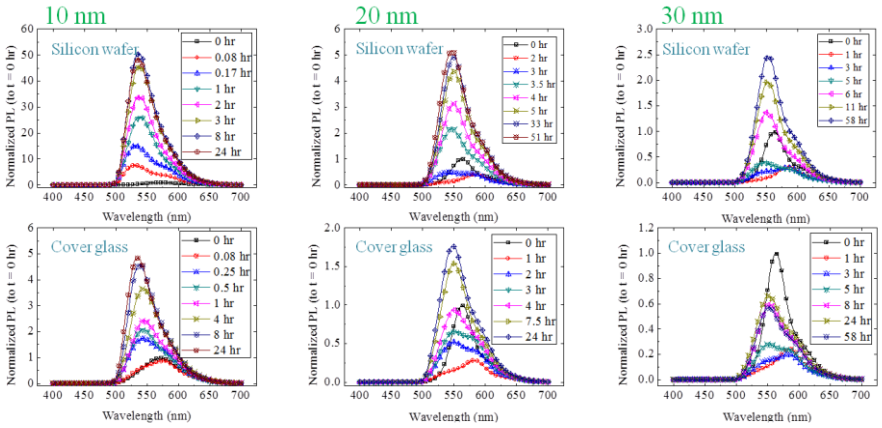

Figure 5. The PL spectra of the MEH-PPV/PS films on either silicon substrate or glass slide under various dewetting condition.

	τ = 10 nm	τ = 20 nm	τ = 30 nm
Si-wafer	ξ = 48.8 folds; $\Delta\lambda$ = 37 nm (573→536 nm)	ξ = 5.2 folds; $\Delta\lambda$ = 15 nm (562→547 nm)	ξ = 2.5 folds; $\Delta\lambda$ = 10 nm (562→552 nm)
SiO_x-wafer	ξ = 3.0 folds; $\Delta\lambda$ = 16 nm (556→540 nm)	ξ = 1.2 folds; $\Delta\lambda$ = 15 nm (560→545 nm)	ξ = 0.6 folds; $\Delta\lambda$ = 14 nm (564→550 nm)
Cover glass	ξ = 4.9 folds; $\Delta\lambda$ = 31 nm (571→540 nm)	ξ = 1.8 folds; $\Delta\lambda$ = 16 nm (564→548 nm)	ξ = 0.7 folds; $\Delta\lambda$ = 14 nm (565→551 nm)

Table 1. The enhancement factor of the PL efficiency induced by the dewetting and the blue shifts for various film thickness and substrates.

The role of the capillary forces were also elucidated in the dewetting pattern and PL enhancement that were driven by different degree of forces when the films were on various substrate (e..g, comparing Si-wafer with glass slide) of which the capillary forces (hence the Hamaker constants) were different.

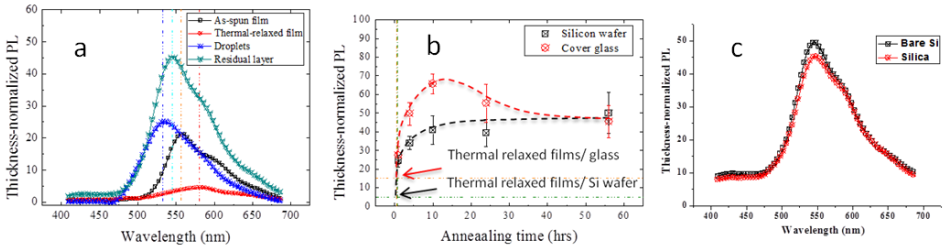

Figure 6. (a) The micro-PL spectra of the MEH-PPV film before dewetting and the local regions of the fully dewetted films, (b) the PL intensity of the micro-PL as recorded as a function of dewetting time for the MEH-PPV films on the various substrates, and (c) the comparison of the micro-PL spectra of the residual layers of the fully dewetted the MEH-PPV films on the Si-wafer and glass slide.

From the PL spectra as acquired from using the confocal micro-PL, the locations where stretched conjugated polymers were located were found to emitd light with much higher efficiencies. The efficiencies of the residual layer increased persistently as the dewetting continued. The polymer chains in the residual layer, highly stretched and constrained, illustrated no exciton quenching even within 2-3 nm on the highly lossy substrate of Si wafer. Almost instantaneous to their first appearance, the residual layer manifests the capability to switch off exciton quenching. Clearly, mechanical stress of sufficient magnitude may switch off the heterojunction quenching that otherwise prevailed in the MEH-PPV/PS film on the Si-wafer before dewetting.

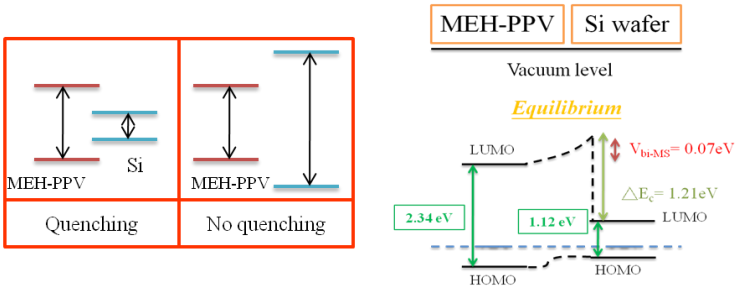

Figure 7. The energy gaps of the MEH-PPV film relative to those of the Si-wafer and glass slide substrates.

B. Dewetting by Solvent Annealing:

The effects of stretching the conjugated polymer of MEH-PPV (Mw = 55kg/mole) on the photoluminescence behavior was further studied in the experiment of solvent annealing when the conjugated polymer was embedded in the ultrathin polystyrene (PS) films (10 nm) of various PS molecular weights (Mw = 2k, 400k, and 1.5Mg/mole). The films were prepared by spin coating the polymer solution in equal-parted toluene, THF and cyclohexanone. The substrate used was either Si-wafer with native oxide (≦ 2 nm) or cover glass.

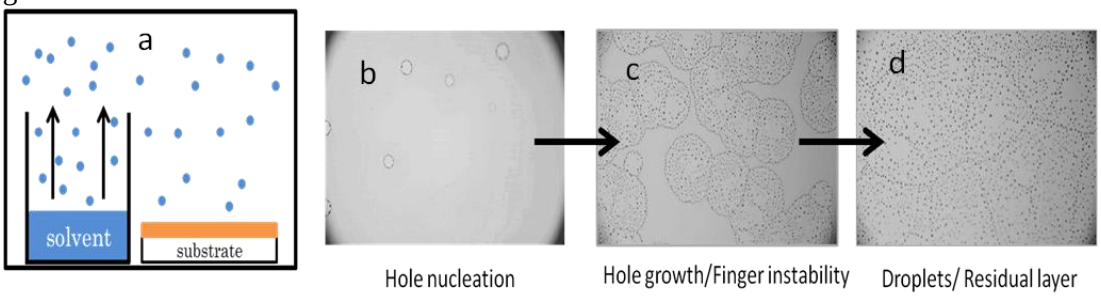

Figure 8. (a) A schematic depiction of the solvent-annealing in an enclosed, temperature-controlled chamber. (b-d) OM micrographs of the solvent-annealed MEH-PPV films undergoing dewetting.

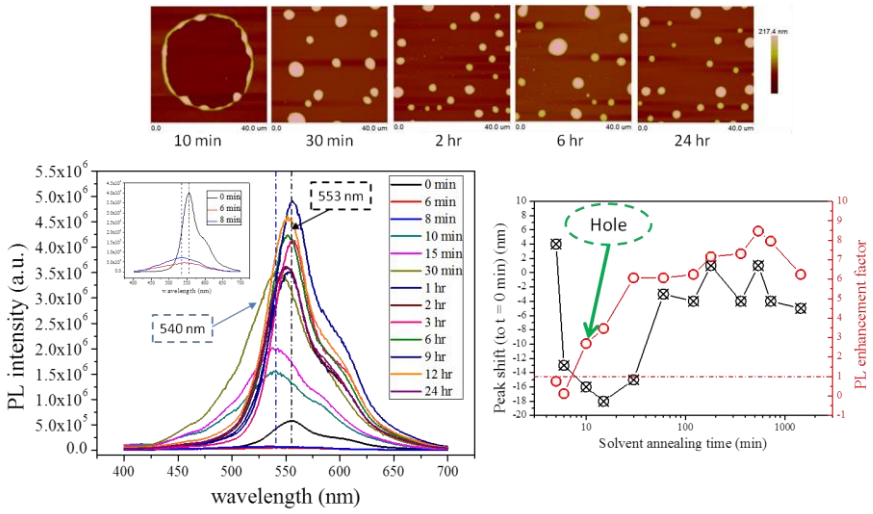

Figure 9. The AFM topographic micrographs, the PL spectra, and the analysis of the PL peak position and intensity as a function of annealing time, for a film of **5%** MEH-PPV/PS in PS (MW=2kg/mol.) that dewetted in the toluene environment.

When imbibed in the solvent vapor enclosed in a chamber, the polymer films underwent dewetting (Fig. 8) after a period of time passing a threshold. The solvent for the annealing was toluene (good solvent) or acetone (poor solvent). The chamber temperature was kept at 30^0C in an oven.

Consistent to that observed in the thermally annealed MEH-PPV films, the solvent-induced dewetted films manifested dramatically increased PL intensity with a blue-shift (~18 nm) (Fig. 9) after the initial decrease of PL intensity (~90% drop) immediately upon solvent annealing before the appearance of the pinholes. However, the initial red-shift observed in the thermal dewetted film, which was attributed to the formation of molecular aggregates, was absent here. It indicates that the plasticizing solvent molecules in the ultrathin film can effectively mobilize the conjugated polymer strands when the residual stress was still operative, but they somehow blocked the direct contact between conjugated chain segments such that molecular aggregation was suppressed.

As revealed by the confocal micro-PL survey, the PL efficiency at the residual layer was extremely strong. It also clearly manifested that in the highly stretched polymer chains could switch off the substrate quenching effect, consistent with what observed in the thermally annealed films (Fig. 6c).

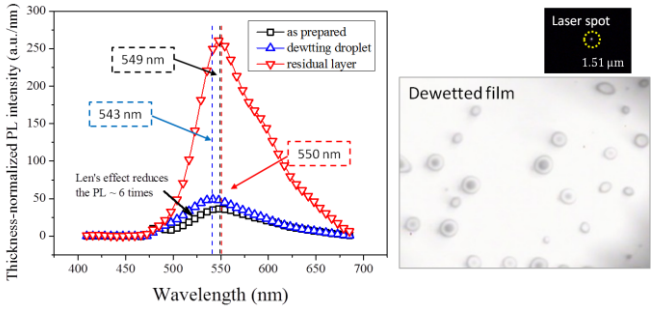

Figure 10. Micro-PL spectra of the as spun film, as well as the droplets and residual layer of the fully dewetted film.

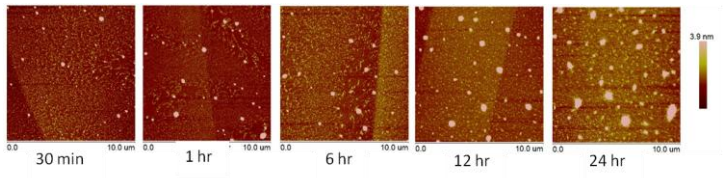

AFM	Thickness	Roughness
30 min	**1.85 nm**	0.51 nm
3 hr	**2.08 nm**	0.35 nm
6 hr	**1.94 nm**	0.41 nm
12 hr	**1.87 nm**	0.51 nm
24 hr	**1.96 nm**	1.07 nm

Consistent

XRR	Thickness
30 min	**1.95 nm**
2.5 hr	**1.83 nm**

Figure 11. The thickness of the residual layer as determined using the x-ray reflectivity and AFM.

The residual layer thickness, as measured by x-ray reflectivity and AFM, was very close to that via thermal dewetting, to be around 2 nm (Fig. 11). As shown by the mass density

distribution in the thickness direction in the ultrathin films before and after the solvent imbibing (Fig. 12), the onset of the molecular flows associated with dewetting required solvent saturation of the whole films down to the substrate surface, as indicated by the vacant regions right next to the substrate in the soaked/dry films for either the good or poor solvent.

	Pre-dewetting		Annealed film (toluene, 6 min)*		Annealed film (acetone, 6 min)*	
	Thickness (nm)	SLD (10^{-6}Å^{-2})	Thickness (nm)	SLD (10^{-6}Å^{-2})	Thickness (nm)	SLD (10^{-6}Å^{-2})
Top	10.53	9.54	10.55	12.99	10.41	10.44
Bottom	1.73	**3.06**	1.62	**0.14**	1.59	**0.12**
Total	**12.3**		**12.2**		**12.0**	

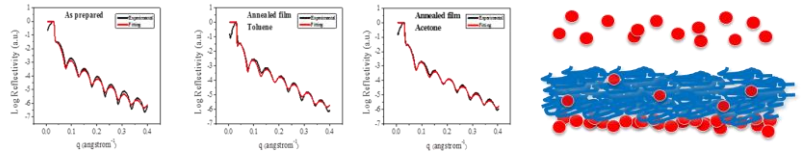

Figure 12. Comparison of mass density distribution (SLD) along the thickness direction in the MEH-PPV/PS films before and after the initial solvent annealing (in both the good solvent toluene as well as the poorer solvent acetone) before the emergence of dewetting pinholes.

The blue shift was the fingerprint associated with the PL enhancement induced by dewetting by thermal annealing. The blue shift, however, was transient for the solvent-annealing induced dewetting (Fig. 13). As illustrated, the poorer solvent induced smaller transient blue shift.

The blue shifts were attributed to the emergence of transient molecular kinks during the molecular flows of dewetting. In good solvent, the MEH-PPV chains were separated by the penetrating solvent molecules and re-entangled during the molecular flows. The re-entanglement created transient molecular kinks, shortening the conjugation length and giving rise to the blue shifts. At long annealing times, these molecular kinks were ultimately relaxed, leading to recovery of the blue shifts. On the other hand, in poor solvent, MEH-PPV retained most of their original chain entanglements due to the weak plasticization of the solvent, hence the transient molecular kinks were fewer and the blue shifts smaller.

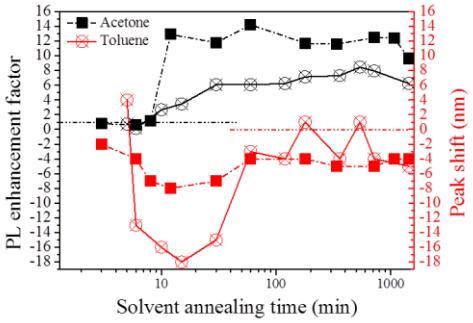

Figure 13. PL enhancement and the blue shifts were illustrated as a function of dewetting time for solvent-annealing using either the good solvent (toluene) or the poor solvent (acetone).

Furthermore, the blue shift was found to increase as the PS chains increase in chain length from 2kg/mol., well below the entanglement molecular weight (M_e ~17.5 kg/mol. for PS), to substantially above, MW= 400kg/mol. and 1.5Mg/mol. (Fig. 15a). Clearly, as the polymer chain becomes longer, more chain entanglements are created in the packed, inter-penetrating chain network. From Gaussian peak fitting (Fig. 15b), the blue shift mainly

came from the intra-chain emission. Obviously, entangling chains were more capable to create molecular kinks during the flows (Fig. 15c).

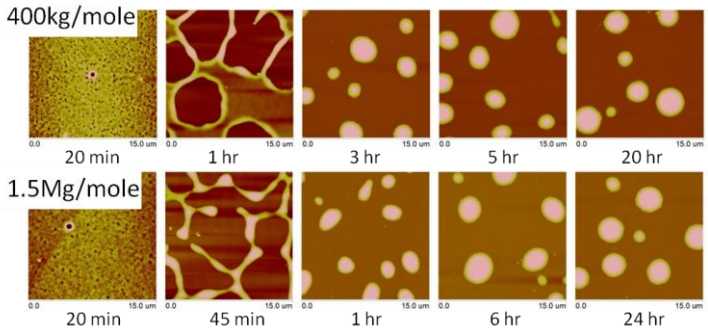

Figure 14. AFM topographic micrographs of the dewetting films, 5% MEH-PPV in the high molecular PS (400kg/mol. and 1.5Mg/mol.), under solvent annealing.

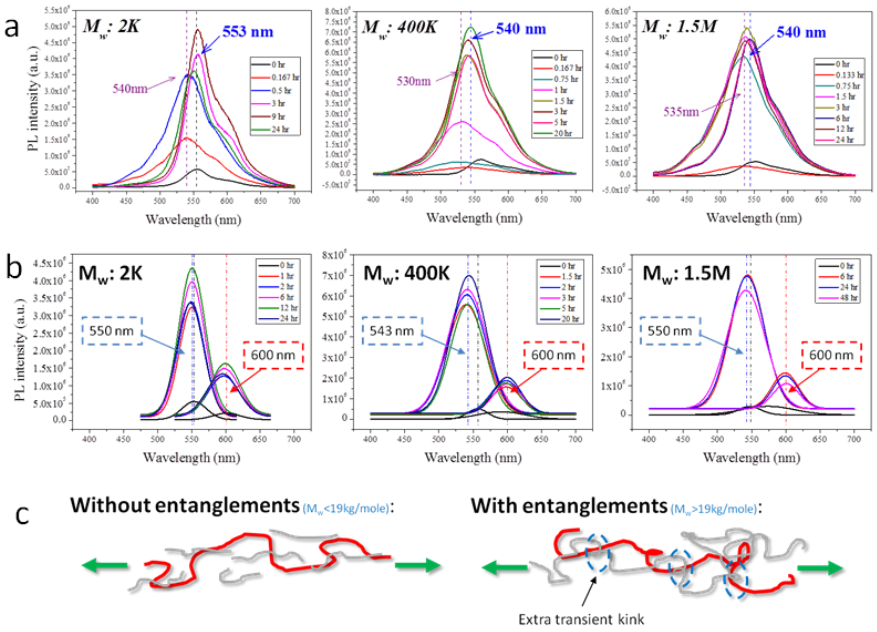

Figure 15. (a,b) Comparison of the PL spectra with different PS molecular weight encompassing the entanglement molecular weight for the original data (a) and the decomposed Gaussian components (b). (c) The proposed chain stretching mechanism for the formation of the molecular kinks via dewetting molecular flows responsible for the blue shifts.

We may conclude here for the solvent dewetting. By using solvent annealing, dewetting instability can be induced to trigger molecular flows that generate sufficient molecular stresses for dramatic efficiency enhancements. The solvent molecules have to penetrate the whole film into the substrate in order to unleash the mechanical instability frozen in the thin films. The residual layer created during the solvent-induced dewetting is essentially similar to that by thermal annealing, in terms of layer thickness and the degree of molecular constraints and optoelectronic enhancements.The blue shifts accompanying the large efficiency enhancements are related to the formation of the transient molecular kinks incurred during the molecular flows.

C. Temperature Effects on the PL Enhancement:

The kinetics of the stress-induced PL enhancements was explored by varying the temperature of the PL measurements. The temperature range probed was from 77K to 300K. The samples were 20 nm thick films (5wt.% of MEH-PPV in 2k PS) before and after dewetting in solvent vapor (toluene or acetone). A confocal optical station was used to allow good spatial resolution for selected area probing. The PLE spectra of MEH-PPV films were recorded using a fluorescent (FP-6300) spectrophotometer. The PL lifetimes were measured by the time-correlated single photon counting (TCSPC) technique (PicoHarp 300, Picoquant). The excitation source is frequency-doubled from a Ti:Sapphire oscillator laser (Tsunami, Spectra Physics) by a 1 mm BBO crystal at 400 nm with 80 MHz repetition rate, coupled with a ADP. For temperature dependent fluorescence spectra measurements, a 406 nm CW laser was used as an excitation source. Fluorescence was collected into a spect rometer (HORIBA Jobin Yvon) with a 1200 l/mm grating and recorded by a cooled CCD (SynapseTM CCD). The spectral resolution of the system is around 0.5 nm. The sample was installed in a cryostat (ST500) with a controllable temperature between 77 and 300 K using liquid nitrogen cooling.

Despite the massive PL enhancment arising from dewetting, the light absorption energy remained unchanged (Fig. 16). This is consistent with the suppression of electron-phonon coupling in the stress-rigidified chains. After dewetting, the temperature dependence decreased drastically, indicating the suppression of the electron-phonon coupling (Fig. 17).

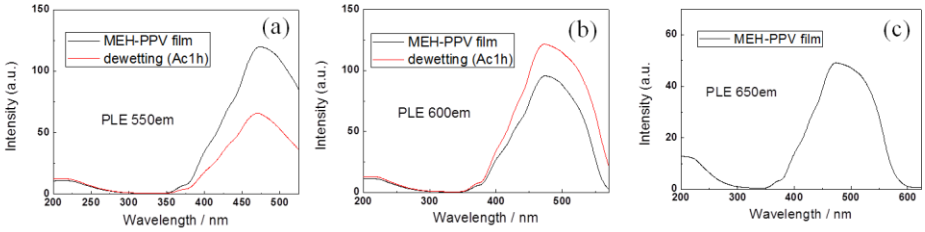

Figure 16. (a,b,c) Fluorescent excitation spectra of MEH-PPV films before and after dewetting (in acetone for 1 hour). PLE were recorded at 550, 600 and 650 nm, respectively.

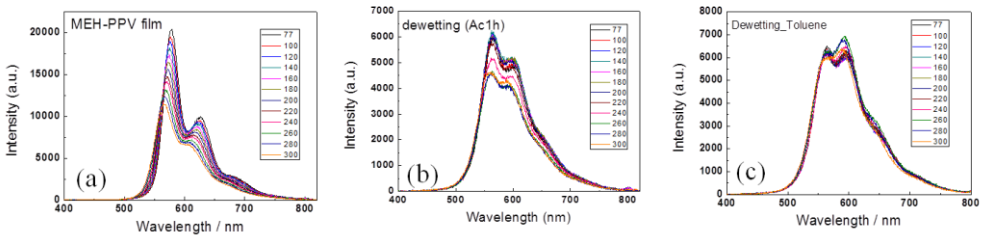

Figure 17. Fluorescence as a function of temperature between 77 K and 300 K for MEH-PPV films (a) before and (b) after dewetting (in acetone of 1 hour). It is evident that the intensity decreases upon an increase in temperature.

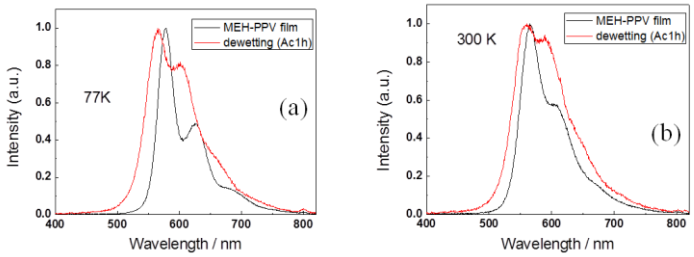

Figure 18. Fluorescent spectra of MEH-PPV films before and after dewetting (in acetone of 1 hour) at (a) 77 K and (b) 300 K.

The width of the PL spectrum (FWHM), a key indicator for the electron-phonon coupling (the Huang-Rhays parameter), became temperature-independent after dewetting (Figs. 20c and 21c), evidently indicating the direct connection of efficiency enhancements and the suppression of the phonon coupling. Undoubtedly, the energy transfer during the de-excitation process in conjugated polymers is altered by mechanical stretching, particularly the intramolecular routes (the band-I), consistent with the results acquired previously.

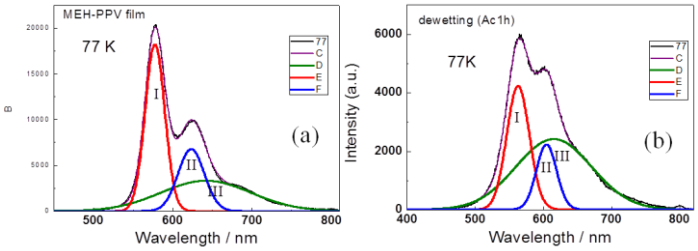

Figure 19. The fluorescence spectrum can be well fitted by a three-Gaussian function. (a) before and (b) after dewetting (in acetone for 1 hour) at 77 K.

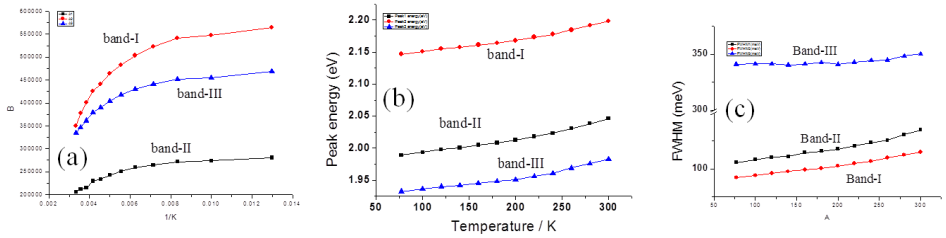

Figure 20. (a) the Arrhenius plot of the fluorescence intensity, (b) the energy gap and (c) the bandwidth for band-I, band-II and the band-III as a function of temperature in MEH-PPV films between 77 K and 300 K.

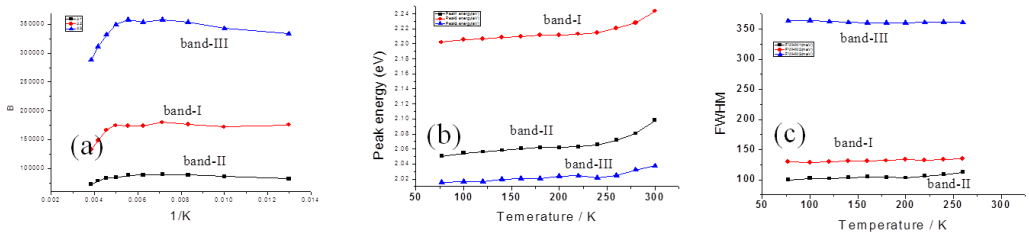

Figure 21. (a) the Arrhenius plot of the fluorescence intensity, (b) the energy gap and (c) the bandwidth for band-I, band-II and the band-III as a function of temperature in MEH-PPV films after dewetting between 77 K and 300 K.

D. Ultrafast Time-Resolved PL of the Dewetted Droplets:

The droplets generated from dewetting under solvent annealing were explored for the PL spectra in the time frame neighboring the mechanical relaxation time constant of conjugated polymers ~200fs. Due to the difficult of measurements, the samples probed were neat MEH-PPV films (100 nm) and fully dewetted films (20 nm) of 20% MEH-PPV in PS (2k).

Generally, the PL intensity decreases quickly with delay time and the PL peak shifts to greater wavelengths, indicating quick damping of excitation energy absorbed from the light. Before dewetting, the PL peak is at ~535 nm for 0.5 ps. However, after the molecular flows

of dewetting, the PL peak for the same delay time is at below 520 nm. For the shortest time below 0.5 ps, the peak appears to be merged with the absorption wavelength (473 nm). Substantially retarded energy damping occurred in the short-time regime when the molecules are stretched.

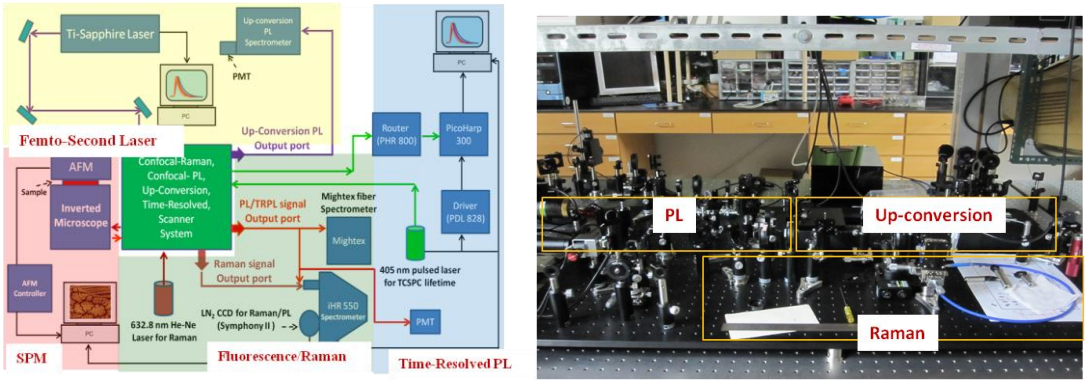

Figure 22. Schematic layout and the photo of the confocal optical systems consisting the ultrafast PL (up-conversion modulus) coupled with an AFM.

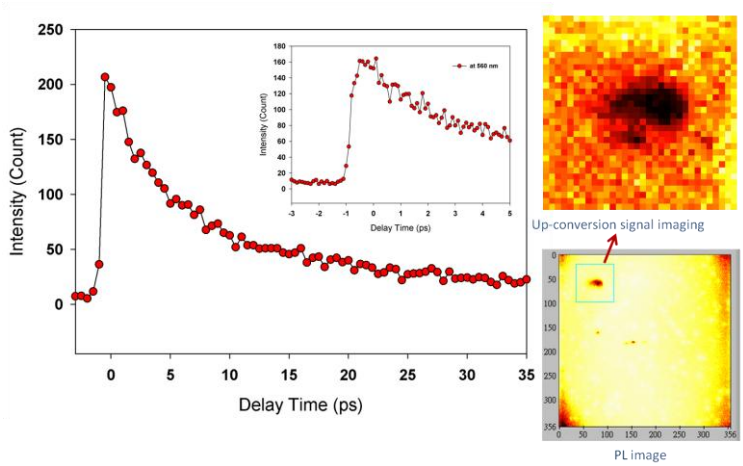

Figure 23. Up-conversion measurements of the 100 nm MEH-PPV film.

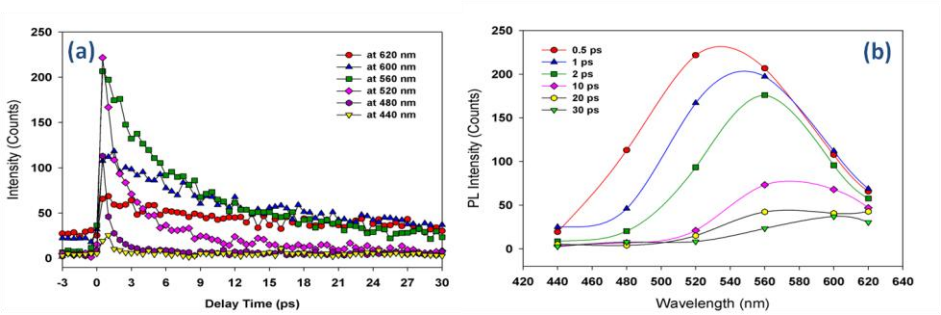

Figure 24. Left: Up-conversion signals of 100 nm MEH-PPV film at different wavelengths. Right: Time-resolved PL spectra of 100 nm MEH-PPV film.

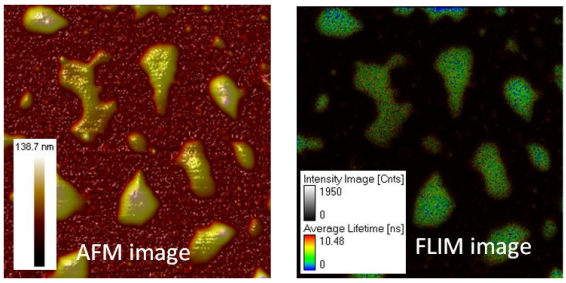

Figure 25. The droplets of the dewetted sample to be explored in the ultrafast PL measurements.

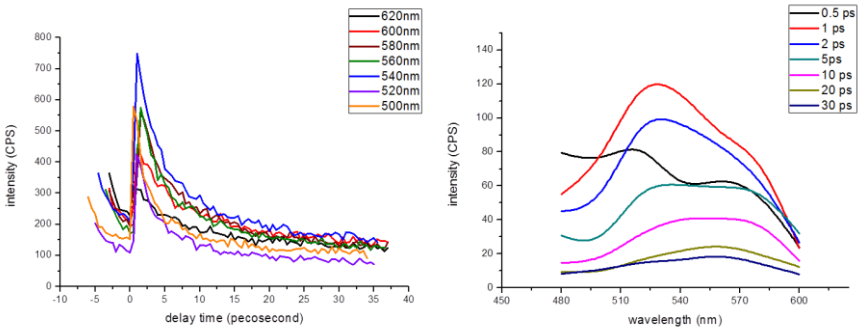

Figure 26. (left) Time-resolved PL spectra of 100 nm MEH-PPV film. (right) Time-resolved PL spectra of a MEH-PPV dewetting droplet.

3. Damped Heterojunction Quenching at Graphene by Mechanical Stretching

Heterojunction quenching has long been understood by annihilation of the excitons that diffuse near the interface of a low-bandgap material where the built-in field tears apart the Coulomb-bound charge pairs. The decrease of heterojunction quenching due to large mechanical stress, as elucidated in the above, is a clear manifestation that the mechanical stresses operative in molecular segments are directly connected to the formation and behavior of the excitons and has put the conventional exciton theory based on Coulomb interactions into doubts. In view of its importance, this effect was sought to be re-confirmed in a new experiment where the mechanical stress was directly applied to the polymer chains by pulling forces, rather than the capillary forces that dictated in the dewetting experiments.

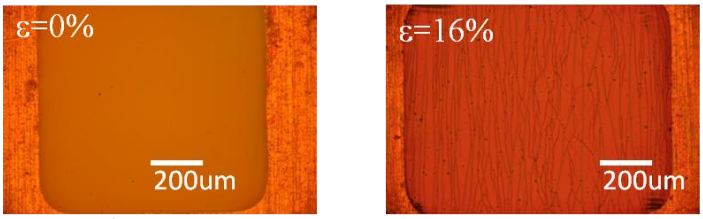

0 % graphene 3.8 wt% graphene

Figure 27. Local deformation zones of crazes developed in the graphene-added MEH-PPV/PS films after mechanical stretching where ε is the tensile strain.

In this experiment, classified small graphene particles were dispersed into the MEH-PPV/PS thin films (~0.4 μm) that were mechanically stretched uni-axially after bonding to a piece of ductile copper grids. After the stretching, local deformation zones of crazes formed (Fig. 27) that clearly demonstrated the micro-necking behavior warranting the determination of the local stress and strain via the Bridgman's plasticity model (Fig. 28).
Before the mechanical stretching, the graphene particles clearly showed a strong quenching

effect in that the PL of the luminescent films decreased substantially with the amount of graphene present in the sample. However, the PL intensity increase due to the mechanical stress was greater in the graphene-added samples (Fig. 29), indicating that the PL quenching by the graphene particles was reduced by the mechanical stretching.

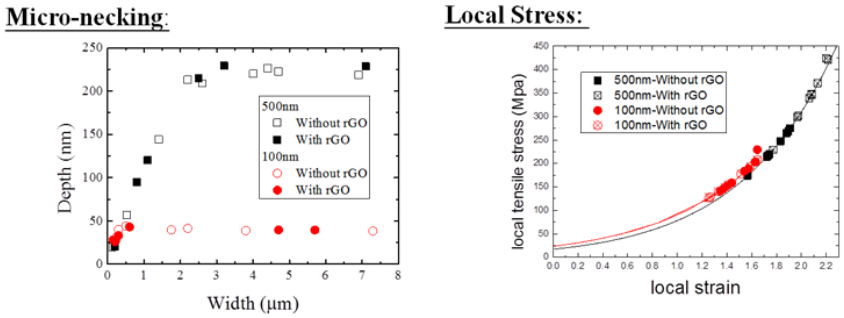

Figure 28. The depth of the crazes versus the craze width clearly demonstrating the micro-necking behavior, based on which, the local stress can be determined by the Bridgman's model.

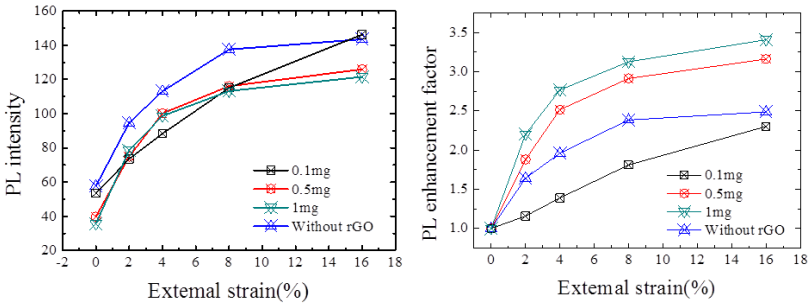

Figure 29. The PL intensity and the enhancement factor versus the external strain for various graphene fractions.

4. Molecular Constraints by Hydrogen Bonding

If stretching polymer chains may rigidify the backbones to achieve massive enhancements of optoelectronic efficiencies via suppression of the electron-phonon coupling, similar results should emerge when inter-molecular hydrogen bonding (HB) were introduced to constrain the polymer backbone. In this report, we try to constrain a conjugated polymer of a backbone of poly(3-hexylthiophene) (P3HT) with hydrogen bonding. Hydrogen bonding (HB) is one of the molecular interactions arising from permanent dipole interactions between the hydrogen atom covalently bonded to an atom (X) and another atom (Y) where both X and Y are both of high electron affinities. The bonding is directional with bonding energy up to ~200 kJ/mol but typically in the range of 5-30 kJ/mol., which is smaller than common covalent bonds, ionic bonds, or metallic bonds, but stronger than van der Waal's forces. It may occur within a single molecule (notably between coplanar hexagonal or pentagonal groups), or inter-molecularly to raise the miscibility between the HB pair of solute and solvent. In addition, since HB forces are greater than the typical polar interactions between molecules and may be easily installed in polymers, it is highly interesting to reveal if HB forces are strong enough to impose sufficient molecular constraints to restrict segmental motions of the polymer segments so that the electron-phonon coupling may be suppressed to increase the optoelectronic efficiencies.

Hence, a conjugated polymer poly 2-(thiophen-3-yl) ethyl acetate (PTEA) (Fig. 30) was synthesized with HB acceptor C=O moiety extended from the side group. The polymer was

so designed such that there are no HB forces in the neat polymer, within or between molecules, unless a diluent containing HB donor groups was dispersed within the conjugated polymer. As will be shown here, the HB between the donor and acceptor increase the miscibility of the blend, rendering the HB forces to be readily controlled by the diluent fraction so that the effect of molecular constraints by HB on the optoelectronic efficiencies of the conjugate polymer can be unveiled. In contrast, another diluent of similar chemical structure but containing no HB donor was also used, as a control, to examine the effect of blending without the HB forces on the photoluminescence properties. We found that very large enhancement in the photoluminescence was observed in the systems prevailed with intermolecular HB forces while the ones without the HB forces manifest only slight improvements of optoelectronic efficiencies arising from dispersion. The results elucidate the important effect of molecular constraints on optoelectronic efficiencies of conjugated polymers and simultaneously outline the sensitivity of the effect on the interaction magnitude as hinted by the HB interactions.

Synthesis of PTEA Monomer and Polymer:

The conjugated polymer (PTEA) with the HB acceptor was synthesized from the monomer 2-(thiophen-3-yl)ethyl acetate (TEA) under the catalysis reaction by anhydrous $FeCl_3$ in chloroform solution. The TEA monomer was obtained from the reaction of 2-(thiophen-3-yl)-ethanol (TE, Aldrich) and acetyl chloride (Aldrich) catalyzed by 4-dimethylaminopyridine (DMAP; Aldrich) and triethylamine (Aldrich), in anhydrous tetrahydrofuran (THF; Aldrich). The diluent containing the HB donor, 4-octylphenol (OP; Aldrich), and the control diluent of no HB interactions, 1-phenyl-1-decanone (PD; Aldrich), were used as received without further purification.

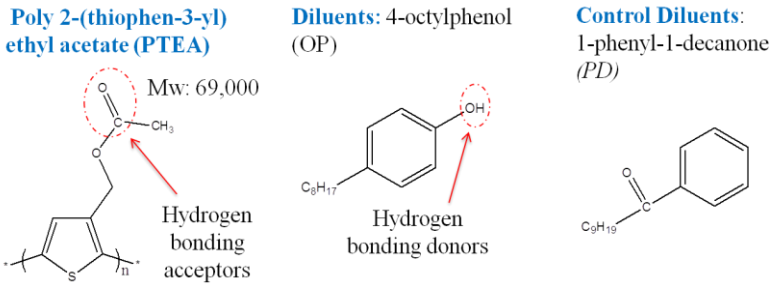

Figure 30. The conjugated polymer PTEA containing the hydrogen bonding acceptor group –C=O, the diluent OP containing the hydrogen bonding donor group –O-H, as well as the small molecule PD that contains no hydrogen bonding group serving as the control diluent.

TE(5 g, 39 mmol), DMAP (0.3 g) and triethylamine (4.55 g, 45 mmol) were dissolved in dry THF (50 mL) and cooled down to 0 ℃ in an ice bath. The solution of acetyl chloride (3. 53 g, 45 mmol,) in dry THF (20 mL) was added gradually into the above solution in 1 h. The mixture was subsequently stirred at 0 ℃ for 3 h, and then raised to 25 ℃ for additional 12 h. Later, after solvent removal via vacuum filtration, the crude product was dissolved in 100 ml of ethyl acetate, washed with aqueous $NaHCO_3$ and brine, and then dried by anhydrous m agnesium sulfate and solvent removal via rotary evaporation. Finally, the residue was purifie d through the chromatography (SiO_2; dichloromethane) to obtain the yellow liquid product (5.94 g, yield = 90%). The scheme showed the synthesis route of the PTEA, TEA monomer and TE in Figure 31 a. The chemical shift of TEA monomer was identified by ^{1}H-NMR and ^{13}C-NMR analysis as shown in Figure 31b.

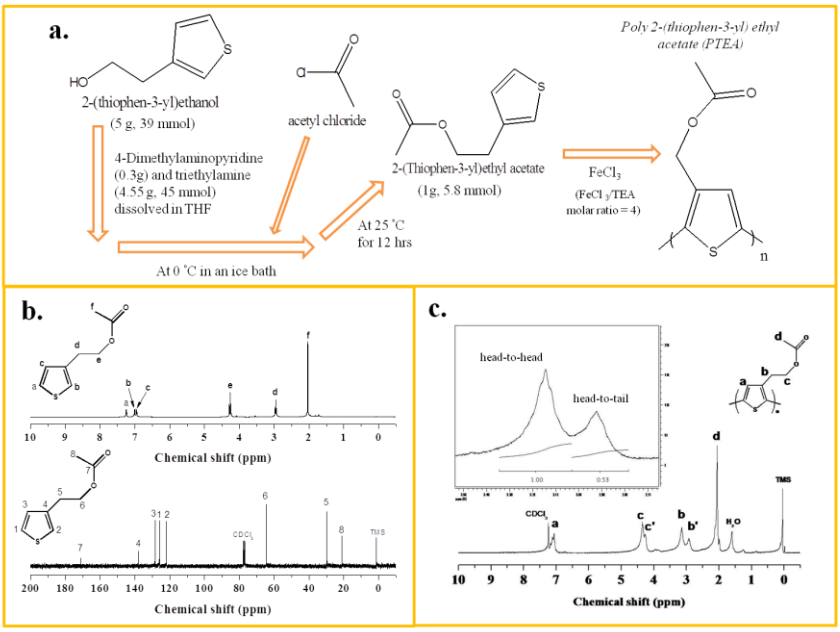

Figure 31. (a) Synthesis route of the PTEA, TEA monomer and TE, (b) H^1-NMR and C^{13}-NMR chemical shift of 2-(thiophen-3-yl) ethanol, (c) H^1-NMR chemical shift of poly 2-(thiophen-3-yl) ethanol.

2-(thiophen-3-yl) ethyl acetate (1g, 5.8 mmol) and anhydrous $FeCl_3$ (3.81 g, 23.5 mmol) were dissolved in dry chloroform (15 mL) and then the solution was purged with dry argon for 10 min. The solution was degassed through three freeze/thaw evacuation cycles. Subsequently, the mixture was reacted for 12h at room temperature and poured into methanol (200 mL) to precipitate the polymers. The crude polymers were filtered, further purified by the extraction in a Soxhlet extractor with refluxing methanol for 48 h, and dried under vacuum to give 0.6 g of 65% regioregular head-to-tail polymers. The regioregularity was calculated from the H^1-NMR spectra by comparing the relative integrations of the signals at chemical shifts of ca. 2.92 [head-to-tail (H-T)] and 3.15 [head-to-head (H-H)] ppm. The chemical shift of PTEA was identified by ^{1}H-NMR analysis as shown in Figure 31c. The nuclear magnetic resonance spectroscopy (^{1}H-NMR and ^{13}C-NMR) spectra were recorded using a Varian Inova 300 MHz Spectrometer equipped with a 9.395 T Bruker magnet and operated at 300 MHz. Samples (ca. 5 mg for ^{1}H NMR) in $CDCl_3$ solvent were analyzed at room temperature. The molecular weight of PTEA was measured from gel permeation chromatography to be 69,000g/mol.

Ultrathin Solid Films:

10 mg PTEA was dissolved in 1g 1,1,2,2-tetrachloroethane (TCE; Showa) at 50°C for 1 hr. Then, the diluents (OP or PD) were added into the PTEA solution and continuously stirred at 50 °C for 0.5 hr. After filtration *via* nylon syringe through a PTFE filter (0.45 μm pores), the solution was spin-coated on silicon wafer (for 20 s), giving solid films of PTEA weight fraction from 100% to 9% and a thickness ~35 nm controlled by adjusting the spin speed around ~3500 rpm.

The morphology of the solid film was surveyed under an optical microscope (Nikon Optiphot-POL instrument) and an atomic force microscope (AFM) (Digital instrument NS3A; tapping mode using under cantilever spring constant of 0.06 N/m). The emission properties were acquired from using a photoluminescence spectrometer (Perkin-Elmer LS55) typically with an excitation wavelength at 450 nm. The glass transition temperature of the solid films was determined using a differential scanning calorimeter (DSC; TA DSC-Q20) in

dry N_2 atmosphere scanned from -90 to 200 ℃ at 20 ℃/min. The crystal morphology of the solid film was obtained by X-ray diffraction (Rigaku D-Max, Ni-filtered Cu Kα radiation λ=0.154 nm, 30 KV, 20 mA) in the range from 5° to 35° under the scan rate of 2°/min.

Film Morphology:

Under AFM, the spin cast films of PTEA/OP that was designed to have the HB interactions manifested smooth film topography and uniform phase for PTEA concentration (*c*) above ~40 wt.% (Fig. 32c). As *c* decreased further, topographic roughening hinting phase separation emerged. The XRD results indicated that the PTEA/OP film was amorphous of a single phase for *c* > 40 wt.% showing no crystalline sharp peaks in the diffraction pattern. As the *c* decreased to 34 wt.% and below, sharp peaks characterizing OP crystals emerged (Fig. 32a). The crystallinity increased readily with the OP fraction until it reached 1 at 100% OP fraction. The absence of the OP crystals for *c* > 40% is attributed to the influences of the HB interactions between the PTEA/OP pairs that suppressed the aggregation and ordering of the OP molecules in the solid films.

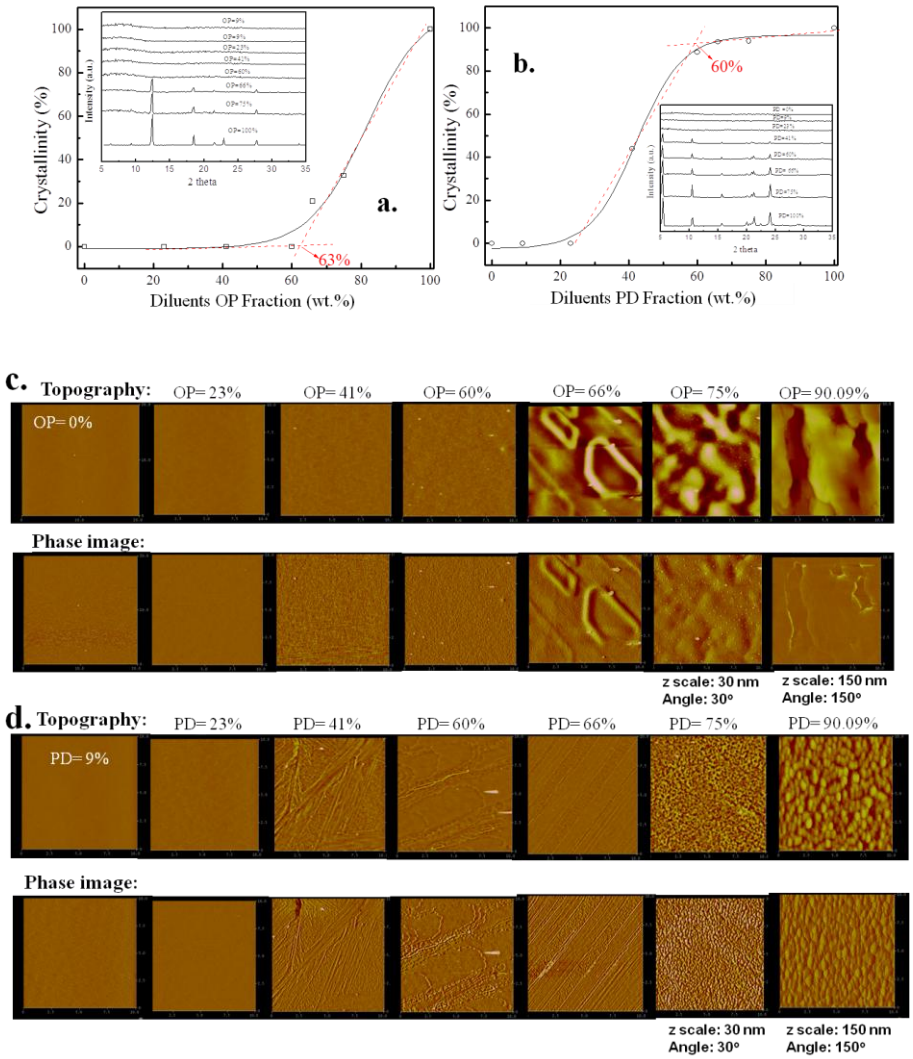

Figure 32. Crystallinity (a) of PTEA/OP blending system, (b) of PTEA/PD blending system (insert is XRD curve), AFM topography and phase images of (c) PTEA/OP solid film and (d) PTEA/PD solid film.

On the other hand, the PTEA/PD system, the control system designed to have no HB

interactions, the films were smooth and uniform for c > 77 wt.% below which topographic roughness increased rapidly (Fig. 32d). Concomitantly, the PD crystallites appeared at above c < 77 wt.% (Fig. 32b). The crystallinity increased with PD fraction and started to saturate at c ~40 wt.%, a deviation (relative to that with the HB interactions) attributed to the molecular packing details in the diluent-rich regime where multiple phases coexisted in the solid films.

Clearly, the HB interactions effectively enhanced the intermolecular interactions between the OP diluent molecules and the conjugated polymer PTEA and hence significantly promoted the dispersion of the molecules.

Emission of Solid Films:

The PL spectra of the PTEA films doped with various c's showed a single prominent PL peak that was shifting to the shorter wavelengths as the diluents concentration (1-c) increased (Fig. 33a). The blue shift readily increased with the diluents concentration and started to saturate as (1-c) approached 70 wt.% at approximately 40 nm (Fig. 33b). Simultaneously, remarkable increases of PL efficiency were observed as the HB interacting diluent (the OP molecules) were added into the conjugated polymer. The efficiency enhancement induced by this intermolecular HB interactions manifested a large period of incubation ~40 wt.% within which the PL efficiency did not change much (Fig. 33b). The efficiency thereafter increased steadily with the OP fraction and started to level off at ~11 folds as OP fraction became greater than ~70 wt.%.

In contrast, the solid films of PTEA that blended with the non-HB interacting diluent PD illustrated only small blue shifts and PL efficiency variations with the diluent fraction. In a d ependence strikingly similar to that of PTEA/OP solid films the blue shift increased with dilu ent fraction up to ~8nm (Fig. 33). The PL increased with PD fraction only up to 2.2 folds.

The emission peak blue shift usually refers to reduction of conjugation length which may be resulted from conjugation disruptions along the polymer backbone or reduction of intermolecular aggregation and energy transfer of the emission processes, in the altered chain packing as consequences of the addition of the diluent.[8-10] In this light, the films of PTEA and OP had manifested far more pronounced diluent effects as compared to the films containing PD diluent, obviously due to the intermolecular HB interactions that had also facilitated diluent dispersion in the conjugated polymer.

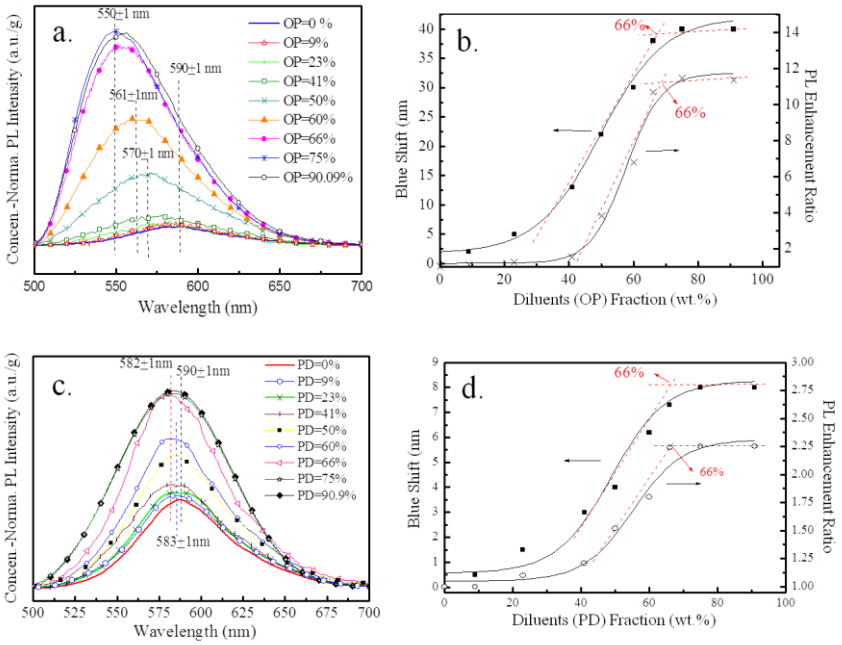

Figure 33. (a) The normalized emission intensity of PTEA/OP system, (b) the peak s

hifted wavelength and the enhancement ratio of PTEA/OP system, (c) the normalized emissi on intensity of PTEA/PD system and (d) the peak shifted wavelength and the enhancement r atio of PTEA/PD system.

Likewise, the PL may be varied due to alterations of the molecular packing. Reduction of intermolecular emission processes arising from the decline of molecular aggregation may lead to increased PL efficiencies, which have been shown in both cases of PTEA with OP and PD diluents. The large differences in the PL efficiencies in these two systems with the PL efficiencies being far greater in the PTEA/OP films, however, are attributed to the additional effect of the intermolecular HB interactions that may effectively constrain the polymer motions and suppress electron-phonon coupling. It is to be clarified, nevertheless, that if the extra increase of the PL efficiencies were simply due to additional chain separation in the HB operative systems of PTEA/OP and not necessarily the additional molecular constraints arising from the HB interactions. Differentiation of the effects of chain separation and constraints are to be revealed by the behavior in the solvent as reported in the following section.

Chain Separation by Diluents:

When dissolved in a solvent (such as TCE), the conjugated polymer PTEA transformed from a molecular packing that manifested rigid chain behavior into solvated flexible macromolecular coils fully permeated with the solvent molecules. In this state, the molecular chains were plasticized rendering exciton trapping more difficult.[16,24] Concomitantly separation between chain segments took place and the inter-chain distances increased with solvent fraction. Consequently, blue shifts of the emission occurred (arising from chain separation)[9-13] amidst the dramatic increase of PL intensity (caused by the plasticization effect). Such behavior was clearly visible, as shown in Figs. 34a and 34b. The blue shift leveled off at c ~1.3 wt.%, consistent with the overlapped chains concentration (c^*) ~1.3 wt.% below which chain separation became constant.[29,30] Notably, the changes in PL efficiencies were enormous, encompassing approximately 6 orders of magnitude, unveiling the massive effect of chain plasticization and exciton trapping prevailing in the conjugated polymer chains packed in solid films.

Also shown in the figures are emission properties when diluent of OP or PD were added into the PTEA liquid solutions. These data converged in the dilute regime with that of the neat PTEA solutions, but deviated sharply for larger PTEA fractions, from the thresholds corresponding to solvent fraction ~10±5 wt%, whilst bounded asymptotically by c, the PTEA fraction in the polymer/diluents mixture. The conspicuous deviations revealed the dissimilar behavior of both diluents relative to the solvent molecules in that the blue shifts were much smaller than those of the neat PTEA in solution in the very concentrated regime where polymer molecules were about to solidify, indicative of far less effective chain separation by the diluent as compared to the solvent. In fact, in terms of molecular separation, the diluent behaved comparable to the polymer molecules as all the blue shift data converged approximately into a master curve when plotted against the total solute concentration in the liquid solution (Fig. 34c). Given so, the maximum blue shifts by solvent in the concentration range corresponding to single-phase solid films (~40 < c < 100 wt.%) (~20 nm) were still substantially smaller than that of the PTEA/OP systems (~40 nm), indicating that the blue shifts observed in the HB pair of PTEA and OP were dominated by factors other than molecular separation. In fact, the blue shift arising from molecular separation in the solid film can be determined of reasonable accuracy from the data of the solutions (Fig. 34a), as will be shown in the following.

Hydrogen Bonding Effects

The dotted line (marked by **A**) depicted in Fig. 34a is the trajectory of the polymer systems – of various weight ratios (~c's) of PTEA versus the diluent – with very tiny

amounts of solvent, although sufficient for polymer plasticization, negligible for contribution to molecular separation. Hence, the blue shifts due to molecular separation by the diluent in the solid films can be estimated from the dotted line **A** showing the primordial film packing. The blue shift due to molecular separation in the solid film was found to increase with the diluent fraction but capped at ~8 nm, a value very close to the maximum blue shift observed in the PTEA/PD systems where no HB interactions were operative. In fact, the blue shifts in the PTEA/PD were overwhelmingly coming from that by molecular separation of the diluent (Fig. 34d). On the other hand, in the PTEA/OP system where HB interactions were implemented between the pair, only a minor part of the blue shift coming from molecular separation whilst the majority was arising from other sources mediated by HB interactions. As will be shown next, it was most likely due to conjugation disruptions arising from the molecular packing mediated by intermolecular HB interactions during the final formation stage of the solid films.

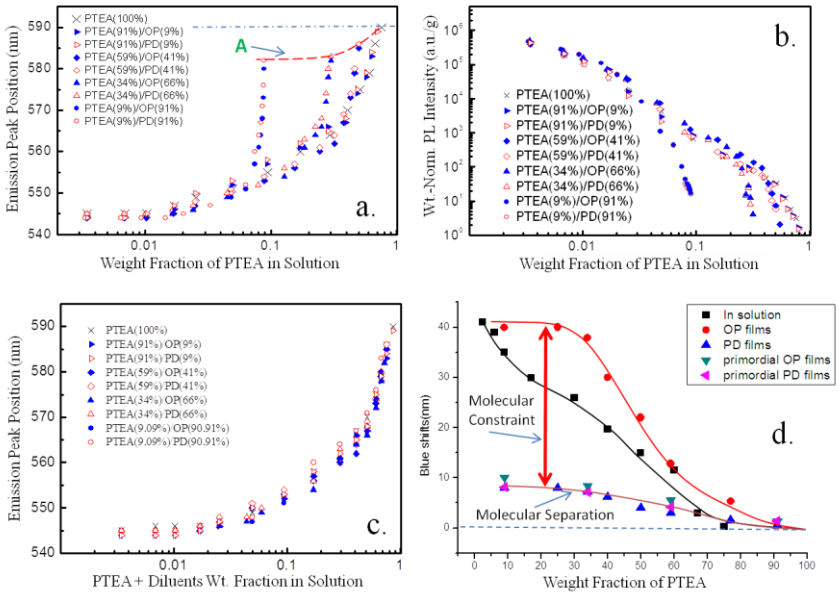

Figure 34. Emission peak wavelength (a) and intensity (b) of PTEA/OP and PTEA/PD versus PTEA weight fraction in the solution. (c) The emission peak wavelength of both PTEA/OP and PTEA/PD versus the solute (PTEA + diluent) weight fraction. (d) The blue shifts of PTEA in solvent and solid films as well as the primordial film packing depicted in the dotted line **A** in (a).

Notably, in the liquid solutions of full concentration range, the diluents OP and PD behaved almost identically in terms of the emission properties of the conjugated polymer, albeit the OP solutions generally illustrated modestly greater blue shifts and stronger PL intensity. This indicates the insignificant effects due to the intermolecular HB interactions for the optoelectronic processes involving solvated conjugated polymer even in the very concentrated regime, in sharp contrast to the substantial role of HB interactions in solid films. It hence manifested that HB interactions are important for the optoelectronic behavior of conjugated polymers only when the polymer chains are packed in solid state when solvent plasticization is negligible.

Furthermore, intriguingly, large increases of blue shift were created during the last leg of solvent evaporation in forming the solid films, to bridge the difference between the primordial packing (dotted line **A,** Fig. 34a) and the solid film (Fig. 34b), at the presence of the HB interactive diluents. Considering that the polymer molecules had well entered into the glassy state and that only tiny amount of solvent (fraction << 1%) was available, this

prominent blue shift cannot result from further molecular separation. Rather, it is likely arising from backbone conjugation disruptions caused by the steric hindrance imposed by the diluents strongly attached to the PTEA chains during the final molecular packing process when the polymer chains were about to pack into the final positions to form the solid film. The conjugation disruptions persisted, as the blue shift leveled off, even in the face of phase separation when excess diluent aggregated to form 2nd phase crystallites. Conversely, without the molecular constraint arising from the HB interactions, the polymer chains may coordinately move smoothly into the final packing positions without incurring substantial backbone conjugation disruptions, hence leaving the blue shift of the solid film comparable to that of the primordial packing.

In addition, with the HB interactions, the diluent was confined to the vicinities of the conjugated polymer chains and hence significantly expanded the single-phase concentration range. On the other hand, without the HB interactions, the diluent segregated to form the 2nd phase at a far lower threshold concentration.

Obviously, the molecular constraints arising from the strong interactions between the HB interactive diluent and the conjugated polymer chain segments may effectively hinder the local molecular deformations typically following optoelectronic excitations, hence suppressing the electron-phonon coupling of the conjugated polymer. This will reduce exciton-trapping and lead to the dramatic enhancements of the optoelectronic efficiencies, as observed in the PTEA films blended with the OP diluent. Relative to the efficiency variations observed in the non-HB interactive diluent PD and PTEA that was attributed to the reduction of intermolecular energy transfer,[31] the enhancement effect due to HB interactions is substantial and may be exploited for optoelectronic applications. It provides a unique example of efficiency enhancements by molecular constraints where the electron-phonon coupling is suppressed using a non-mechanical in-situ method.

5. Imprinting

Imprinting is a common method to introduce local deformation regions to a thin polymer film. If these local deformed regions can have the effect of enhanced optoelectronic efficiencies as that demonstrated by mechanically stretched polymers, we can then use this method to manipulate the local optoelectronic properties of thin films and consequently to make efficiency-enhanced optoelectronic devices based on polymers.

The initial data clearly showed that nanoimprinted sample can deliver enhanced PL efficiency (Fig. 35). However, large error bars and stress relaxation effects appeared to influence significantly the subsequent experimental progress and the work was continued into the next year. More complete results will be presented in the next report.

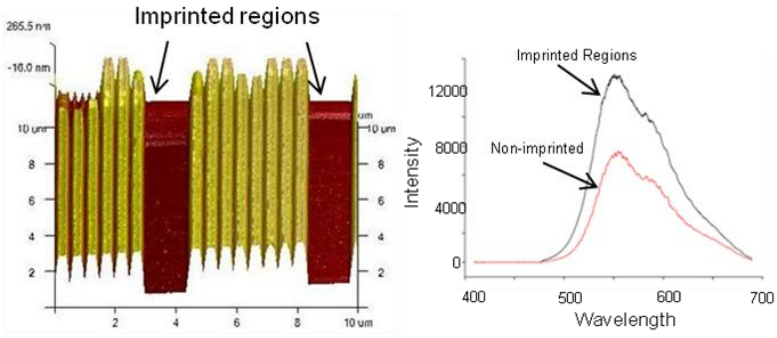

Figure 35. Nanoimprinted MEH-PPV/PS film exhibits enhanced PL efficiency.

Conclusions:

We may conclude for the work performed here. Additional experiments have confirmed the strong effects of molecular stresses on the conjugated polymers that lead to dramatic increases of optoelectronic efficiencies and electric conductivity, as well as longer service life. The length scales of these stress effects are on the order of 10 nm, truly the molecular segmental scales. Fully stretched and constrained conjugated polymer strands exhibit no exciton quenching, indicating the formation and behavior of excitons generated in conjugated polymer are strongly influenced by mechanical stresses and deformations. The stress effect on the electron-phonon interactions may be possibly explored by the ultrafast regime exploration. Intermolecular hydrogen bonding can be used to constrain conjugated polymer strands for highly enhanced efficiencies. One of the keys to major efficiency breakthrough in conjugated polymers may lie in the success of exploitation of this stress effect for practical applications and thus worth further research both technologically and fundamentally.

Acknowledgements:

I would like to thanks the contribution of my graduate students: Peiwei Lee, Po-Tsun Chen, Chih Hung Chang, Wei-Cheng Li, Chi-Ching Liu, Po-Yan Peng, Orlando Marin, and Ya-Wei Yang. I also owe the help of my collaborators: Prof. Gunter Reiter of the University of Freiburg, Germany, Prof. F. C. Chang, of the National Chiao-Tung University, Hsinchu, Taiwan, Prof. J. D. White of the Yuan Ze University, Taiwan, Dr. J. H. Tang and Dr. Ping Yu of the Center of Applied Science, National Academic Sinica, Taipei, Taiwan, Dr. Chein-Chung Chen of the Instruments Center, National Tsing Hua University, Hsinchu, Taiwan, and Prof. J. H. Jou, Department of Materials Science and Engineering, National Tsing Hua University, Hsinchu, Taiwan.

I greatly appreciate the financial supports by the US Air Force under the Taiwan-US Air force Nanoscience Program (AOARD-12-4064), National Science Council of Taiwan (NSC 100-2120-M-007-001 through -003, and NSC 101-2221-E-007-040-MY3). In addition, a grant from NSC for 2012 Instrument Center SPM Renewal Project as well as a special fund from NTHU for the ultrafast laser equipment are thanked and acknowledged.

List of Publications:

1. P. Lee, W.-C. Li, B.-J. Chen, C.-W. Yang, C.-C. Chang, I. Botiz, G. Reiter, T.-L. Lin, J. Tang, A. C.-M. Yang, 2013**,** "Massive Enhancement of Photoluminescence through Nanofilm Dewetting", *ACS Nano* **7**, 6658-6666.
2. I. Botiz, P. Freyberg, N. Stingelin, A. C.-M. Yang, G. Reiter, 2013, "Reversibly Slowing Dewetting of Conjugated Polymers by Light", *Macromolecules* **46**, 2352.
3. P.-J. Chen, M.-K. Wang, J.-H. Hsu, A. C.-M. Yang, J. D. White, 2013 "Observing and Modeling Light Propagation in Polymer Films", *Appl. Phys. Lett.* **102**, 143302.
4. T.-M. Huang, J.-Y. Lin, L. A. Phuong, C.-N. Liao, W.-T. Whang, A. C. -M. Yang, 2013, "Ultra-Low Resistivity of Charge Transport in Ultrathin Polymer Films", in submission.
5. Y. L. Chang, Y. Chien, G. Reiter, A. C.-M. Yang, 2013, "Molecular Packing of Long Polymer Chains in Ultrathin Films via Spin Casting", in submission.

Patent applications:

1. Arnold C.-M. Yang，" Method for Manufacturing a Polymer Molecular Film for

photo-electronic device"，Taiwan patent granted (I 425695); US patent granted (Patent No.: US8,349,141 B2), Date of Patent: Jan. 8, 2013.

2. C. C. Chen, P. T. Chen, A. C.-M. Yang, "Method for enhancing the efficiencies of conjugated polymers", Taiwan patent application, application number: 100130540; China patent application, application number: 100144720; US patent application, application number: 13/417,776.

DD882 as a separate document was complete.